ARTICLE

OPEN

Minimal unlinking pathways as geodesics in knot polynomial space

Xin Liu [1], Renzo L. Ricca [2,3 ✉] & Xin-Fei Li[4]

Physical knots observed in various contexts – from DNA biology to vortex dynamics and condensed matter physics – are found to undergo topological simplification through iterated recombination of knot strands following a common, qualitative pattern that bears remarkable similarities across fields. Here, by interpreting evolutionary processes as geodesic flows in a suitably defined knot polynomial space, we show that a new measure of topological complexity allows accurate quantification of the probability of decay pathways by selecting the optimal unlinking pathways. We also show that these optimal pathways are captured by a logarithmic best-fit curve related to the distribution of minimum energy states of tight knots. This preliminary approach shows great potential for establishing new relations between topological simplification pathways and energy cascade processes in nature.

[1] BDIC and Institute of Theoretical Physics, Beijing University of Technology, 100 Pingleyuan, Beijing 100124, P.R. China. [2] Department of Mathematics & Applications, Università Milano-Bicocca, Via Cozzi 55, 20125 Milano, Italy. [3] BDIC, Beijing University of Technology, 100 Pingleyuan, Beijing 100124, P.R. China. [4] School of Science, Guangxi University of Science and Technology, 268 Donghuang Street, Liuzhou, Guangxi 545006, P.R. China. ✉email: renzo.ricca@unimib.it

Physical knots observed in various contexts, such as DNA biology[1,2], vortex dynamics[3], and condensed matter physics[4,5] are found to undergo topological simplification by following a common, qualitative pattern that brings complex structures to gradually degenerate to form simpler configurations till final production of small, unlinked, unknotted loops (see the trefoil knot evolution of Fig. 1a and the Hopf link cascade of Fig. 1b). The generic feature that characterizes the cascade process originates in the iterated recombination of knot strands through reconnection events that bear remarkable similarities across fields. The process of topological simplification that brings complex knots to simpler ones in a step-wise manner was first observed[1] in the analysis of site-specific recombination action on DNA catenanes (see Fig. 2a). Surprisingly, similar unlinking patterns were then observed also in classical vortex dynamics, superfluids, and condensates[6,7].

The universality of this process is rooted in the identical geometric mechanism that governs the change of topology of physical filaments[8–12], that through an iterated sequence of single, anti-parallel reconnection events[13] (schematically represented in Fig. 2b) governs the topological cascade pattern of Fig. 2a. Topological changes were quantified by adapted HOMFLYPT polynomials derived from helicity by Liu and Ricca[14] analyzing a family of torus knots and links (denoted by $\{T(p,q)\}$) given by knots/links wrapped on a mathematical torus p times in the longitudinal direction and q times in the meridian direction. It was found that the unlinking sequence of Fig. 2a can be described by a monotonic decreasing sequence of numerical values that matches the observed decrease in topological complexity. The untying sequence of Fig. 2a, however, is not unique. A given knot type, for instance the torus link with six minimum number of crossings denoted by $T(2,6)$ in that sequence, can gradually unlink to the same final end-state, say the unknot $T(2,1)$ (with topological crossing number zero), following pathways different from the one shown in Fig. 2a. So, what makes a given pathway a privileged route towards topological decay has yet to be understood, and even though this may well depend on the particular physical process, a general guiding principle is still lacking.

In order to make progress an extensive search on all possible routes that reduce topologically a given knot to the unknot under certain assumptions has been carried out by Stolz et al.[2] by analyzing hundreds of cases. A summary of the last, most probable stages starting from the torus link $T(2,6)$ is shown in the diagram of Fig. 3, where knot types are pictorially represented by standard minimal presentations[15,16]. In terms of possible transitions the diagram is by no means exhaustive, but it gives an idea of the most probable, alternative routes that $T(2,6)$ can follow by a sequence of single reconnection events towards the unknot $T(2,1)$. Note that the lowest branch of this diagram corresponds to the sequence of Fig. 2a, but what makes this very sequence special is not quite clear. The values computed by Liu and Ricca's adapted polynomial are not so helpful either, since all the numerical sequences obtained from the other alternative routes are equally monotonic decreasing. Some sort of selective principle has been devised by Stolz et al. by computing a probability value for each topological transition given by a single reconnection event represented in Fig. 3 by a long, black arrow. Computation of these values, however, relies on a rather sophisticated machinery based on various assumptions and a combined use of topological analysis and simulations data.

This has prompted us to propose a far simpler, and intriguingly new scenario based on the interpretation of the sequences of Fig. 3 as geodesic flows in a knot polynomial space. By relying on Arnold's original idea[17] of interpreting evolutionary processes as geodesic flows in appropriate metric spaces we propose to identify decaying patterns of topological simplification with geodesic flows in a knot polynomial space. In general this knot space can be viewed as a manifold defined by knot types, whose points are determined by the relative knot polynomials. Since we refer to physical knots, we make use of the adapted polynomials introduced by Liu and Ricca[18,19] to quantify the topology of fluid knots. This is done by taking standard Legendre polynomials to construct a basis and an appropriate metric to compute distance using knot polynomials. This allows to measure and compare geodesic distances between knot types, define and compute relative probabilities, and relate minimal pathways to lower bounds given by minimum energy states[20–22].

In the next section we introduce this space, define an appropriate metric by means of Legendre polynomials, identify the knots by adapted Jones polynomials, compute relative deviation
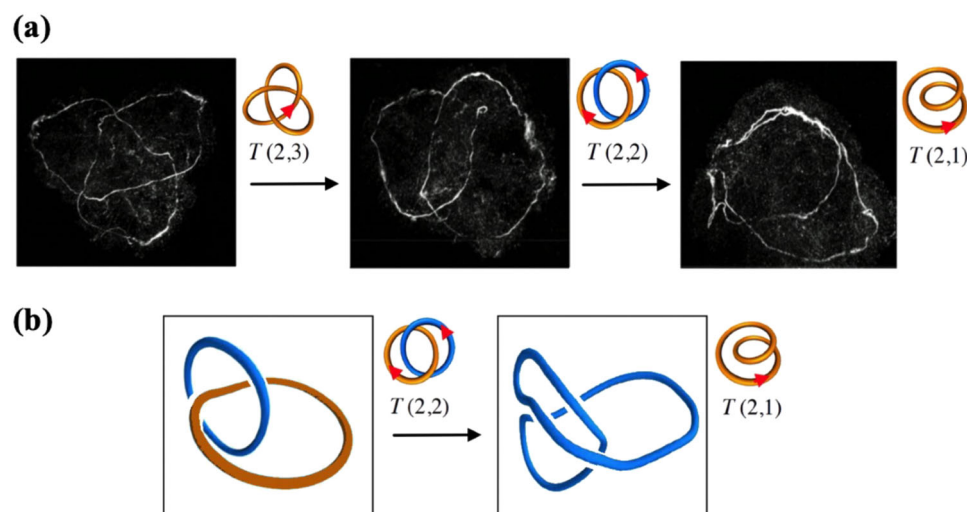
Fig. 1 Topological decay of fluid knots. a Time evolution of reconnecting trefoil vortex in water (snapshots taken, with permission, from Supplementary movies 5 and 6 in ref. [3]). **b** Time frame simulations of Hopf link defects in condensate[5]. Each stage is characterized by the topology of a torus knot or link represented pictorially by the corresponding minimal diagram presentation shown aside. Each torus knot/link $T(p,q)$ is identified by the numbers p and q, denoting, respectively, the number of longitudinal and meridian wraps of the knot/link type on the mathematical torus. Red arrows denote vector field orientation (in this case vorticity), long black arrows topological transitions due to a single reconnection event.
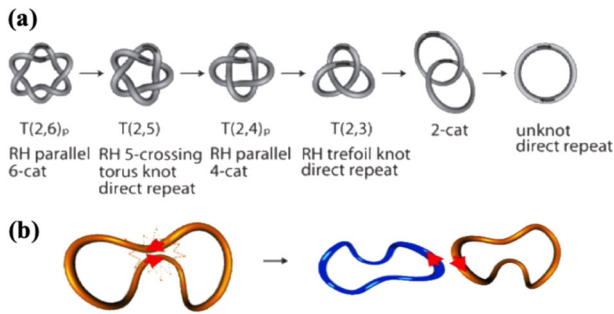
Fig. 2 Topological transition by reconnection event. a Minimal unlinking sequence representing iterated site-specific recombination action on DNA catenanes (taken from ref. [1]). Each torus knot/link $T(p,q)$ is identified by the numbers p and q, denoting, respectively, the number of longitudinal and meridian wraps of the knot/link type on the mathematical torus; RH stands for right-hand knot/link and c-cat denotes catenanes with topological crossing number c_{min}. Long black arrows denote topological transitions due to a single recombination event. **b** Schematic representation of topological transition due to a single, anti-parallel reconnection of knot strands. Red arrows denote strand orientation and long arrow topological transition.

and probability, and provide a comparative analysis between our results and the results obtained by Stolz et al.[2]. We find that the data obtained by our approach match very well the data obtained by the other method, suggesting that the alternative method based on use of geodesics in knot polynomial space has great potential for probability computation of decaying processes of physical systems, even far more complex than the one considered here. By using a new measure of topological complexity based on distances in the knot space we also show that the decaying patterns observed are captured by a logarithmic best-fit curve that is functionally related, and bounded from below, by the logarithmic distribution of minimum energy states of tight physical knots[21,22].

Results

Knot polynomial space. Since all prime knots with nine or fewer crossings have distinct Jones polynomials, for the purpose we have in mind the Jones polynomial $V_K(x)$ (x polynomial variable) provides a sufficiently robust knot identifier. So let us consider the Liu and Ricca adapted Jones polynomial for fluid knots[18], and restrict ourselves to the single variable polynomial with positive exponents of highest degree n. Let us introduce the knot polynomial space $\mathcal{V}_n^+$ according to the following

Definition 1 (Knot polynomial space). The knot polynomial space $\mathcal{V}_n^+$ is an n-dimensional, discrete, Euclidean space endowed by Euclidean metric (to be defined below), whose isolated points (singletons) are the Jones polynomial of knot and link types.

Each singleton in $\mathcal{V}_n^+$ represents a specific knot or link K through its Jones polynomial $V_K(x)$. Let us take the unknot $T(2,1)$ as the origin of $\mathcal{V}_n^+$ given by $V_{T(2,1)} = 1$ (the Jones polynomial value of the unknot). Topological complexity is thus graded by the discrete topology given by iso-complexity level sets $\chi_{c_{min}}$ given by the topological crossing number c_{min}, so that knots/links of same c_{min} lie on the same $\chi_{c_{min}}$-set. Optimal unlinking paths, such as that represented by Fig. 2 (top row), can be interpreted by piece-wise linear geodesic flows in $\mathcal{V}_n^+$ through the level sets $\chi_{c_{min}} = $ constant.

Metric by Legendre polynomials. In order to determine optimal pathways we must make use of an appropriate orthonormal metric. Since the discrete set of points in $\mathcal{V}_n^+$ are given by knot
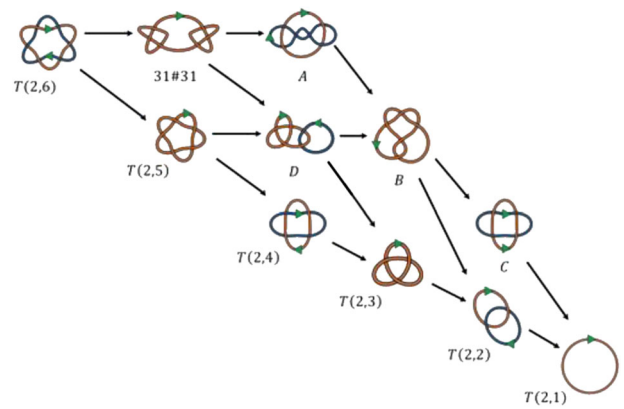
Fig. 3 Alternative unlinking pathways. Paths from torus link $T(2,6)$ to the unknot $T(2,1)$ (diagram adapted from ref. [2]). Each torus knot/link is denoted by $T(p,q)$, where the numbers p and q denote, respectively, the number of longitudinal and meridian wraps of the knot/link type on the mathematical torus. Knot/link representatives denoted by A–D correspond to the Thistlethwaite link notation $L6a1$ (mirror), 5_2, $L4a1$ (anti-parallel), and $T(2,3)\#L2a1$ in the Rolfsen table; $Lc_{min}a1$ stands for link with topological crossing number c_{min} in table position 1, 5_2 denotes knot with topological crossing number $c_{min} = 5$ in table position 2, and $T(2,3)\#L2a1$ the connected sum of trefoil knot (the first torus knot) $T(2,3)$ and Hopf link (the first torus link) $L2a1$, also denoted by $T(2,2)$; 31#31 denotes the composite knot made of two trefoil knots $T(2,3)$ (see ref. [28] for standard knot table and notations). The bottom branch of the diagram represents the minimal unlinking sequence representing iterated site-specific recombination action on DNA catenanes. Green arrows denote strand orientation, long black arrows topological transitions due to single recombination event.

polynomials, for such a metric we must consider the inner product of polynomials $P_n = P_n(x)$ and $P_m = P_m(x)$ in the real variable x. In general this is given by

$$\langle P_n, P_m \rangle = \int_a^b P_n(x) P_m(x) \rho(x) \, \mathrm{d}x, \qquad (1)$$

where a and b are finite, real values, with $\rho(x)$ density function. Orthogonality (together with other mathematical properties) is ensured by a class of standard hyper-geometric polynomials (Jacobi polynomials), widely used in mathematical physics to construct solutions to second-order linear, ordinary differential equations[23]. These, defined through the hyper-geometric function, are given by

$$P_n^{(\alpha,\beta)}(x) = \frac{\Gamma(\alpha + n + 1)}{n! \Gamma(\alpha + \beta + n + 1)} \sum_{m=0}^n \binom{n}{m}$$
$$\frac{\Gamma(\alpha + \beta + n + m + 1)}{\Gamma(\alpha + m + 1)} \left(\frac{x-1}{2} \right)^m, \qquad (2)$$

where $\Gamma(n) = (n-1)!$ for any positive integer n. Orthogonality condition of Jacobi polynomials is given by

$$\langle P_n, P_m \rangle_J = \int_{-1}^1 (1-x)^\alpha (1+x)^\beta P_n^{(\alpha,\beta)}(x) P_m^{(\alpha,\beta)}(x) \, \mathrm{d}x$$
$$= \frac{2^{\alpha+\beta+1}}{2n + \alpha + \beta + 1} \frac{\Gamma(\alpha + n + 1)\Gamma(\beta + n + 1)}{\Gamma(\alpha + \beta + n + 1)n!} \delta_{nm},$$
$$(\alpha > -1, \beta > -1), \qquad (3)$$

where δ_{nm} denotes the standard Kronecker delta. The simplest case is given by taking the density function $\rho(x) = 1$, so that one

Table 1 Legendre coordinates of knots and links in the decay from T(2,6) to T(2,1).

Coordinate	T(2,1)	T(2,2)	T(2,3)	T(2,4)	T(2,5)	T(2,6)	31 # 31	A	B	C	D
c_0	1.4	-5.78×10^1	-6.07×10^2	-9.67×10^3	-1.55×10^5	-2.61×10^6	8.31×10^5	-3.35×10^5	-2.40×10^4	-1.86×10^3	6.07×10^4
c_1	0	-5.35×10^1	-7.40×10^2	-1.27×10^4	-2.16×10^5	-3.77×10^6	1.20×10^6	-4.77×10^5	-3.25×10^4	-2.28×10^3	8.35×10^4
c_2	0	-2.18×10^1	-4.70×10^2	-9.57×10^3	-1.82×10^5	-3.41×10^6	1.07×10^6	-4.15×10^5	-2.55×10^4	-1.50×10^3	6.81×10^4
c_3	0	-4.80×10^0	-1.91×10^2	-5.05×10^3	-1.13×10^5	-2.36×10^6	7.32×10^5	-2.72×10^5	-1.44×10^4	-6.52×10^2	4.04×10^4
c_4	0	-5.46×10^{-1}	-5.17×10^1	-1.96×10^3	-5.45×10^4	-1.31×10^6	3.98×10^5	-1.41×10^5	-6.07×10^3	-1.97×10^2	1.83×10^4
c_5	0	-2.53×10^{-2}	-9.29×10^0	-5.68×10^2	-2.07×10^4	-5.97×10^5	1.75×10^5	-5.83×10^4	-1.95×10^3	-4.20×10^1	6.46×10^3
c_6	0	0	-1.06×10^0	-1.22×10^2	-6.25×10^3	-2.24×10^5	6.29×10^4	-1.94×10^4	-4.80×10^2	-6.15×10^0	1.77×10^3
c_7	0	0	-7.00×10^{-2}	-1.94×10^1	-1.50×10^3	-6.93×10^4	1.84×10^4	-5.21×10^3	-8.96×10^1	-5.93×10^{-1}	3.79×10^2
c_8	0	0	-2.02×10^{-3}	-2.18×10^0	-2.82×10^2	-1.77×10^4	4.40×10^3	-1.12×10^3	-1.25×10^1	-3.39×10^{-2}	6.23×10^1
c_9	0	0	0	-1.66×10^{-1}	-4.15×10^1	-3.74×10^3	8.52×10^2	-1.93×10^2	-1.25×10^0	-8.71×10^{-4}	7.73×10^0
c_{10}	0	0	0	-7.66×10^{-3}	-4.65×10^0	-6.47×10^2	1.32×10^2	-2.59×10^1	-8.59×10^{-2}	0	7.00×10^{-1}
c_{11}	0	0	0	-1.61×10^{-4}	-3.83×10^{-1}	-9.04×10^1	1.62×10^1	-2.67×10^0	-3.59×10^{-3}	0	4.36×10^{-2}
c_{12}	0	0	0	0	-2.19×10^{-2}	-1.01×10^1	1.53×10^0	-2.04×10^{-1}	-6.93×10^{-5}	0	1.67×10^{-3}
c_{13}	0	0	0	0	-7.75×10^{-4}	-8.73×10^{-1}	1.08×10^{-1}	-1.08×10^{-2}	0	0	2.98×10^{-5}
c_{14}	0	0	0	0	-1.28×10^{-5}	-5.67×10^{-2}	5.32×10^{-3}	-3.57×10^{-4}	0	0	0
c_{15}	0	0	0	0	0	-2.60×10^{-3}	1.64×10^{-4}	-5.50×10^{-6}	0	0	0
c_{16}	0	0	0	0	0	-7.47×10^{-5}	2.36×10^{-6}	0	0	0	0
c_{17}	0	0	0	0	0	-1.10×10^{-6}	0	0	0	0	0

c_i denotes the ith Legendre coordinate $i = 1, ..., 17$. Each torus knot/link is denoted by $T(p,q)$, where the numbers p and q denote, respectively, the number of longitudinal and meridian wraps of the knot/link type on the mathematical torus. Knot/link representatives denoted by A–D correspond to the Thistlethwaite link notation L6a1 (mirror), 5_2 L4a1 (anti-parallel) and T(2,3)#L2a1 in the Rolfsen table; $L_{c_{min}}$a1 stands for link with topological crossing number c_{min} in table position 1, 5_2 denotes knot with topological crossing number $c_{min} = 5$ in table position 2, and T(2,3)#L2a1 the connected sum of trefoil knot (the first torus knot) T(2,3) and Hopf link (the first torus link) L2a1, also denoted by T(2,3). 31#31 denotes the composite knot made of two trefoil knots T(2,3) (see ref. 28 for standard knot table and notations).

recovers the special family of Legendre polynomials, with

$$\langle P_n, P_m \rangle_L = \int_{-1}^{1} P_n(x) P_m(x) \, dx = \frac{2}{2n+1} \delta_{nm}, \qquad (4)$$

which determines a complete set of polynomials up to a scale factor. In order to have a unit norm, we must then set

$$L_n(x) = \sqrt{\frac{2n+1}{2}} P_n(x), \qquad (5)$$

so that

$$\int_{-1}^{1} L_n(x) L_m(x) \, dx = \delta_{nm}. \qquad (6)$$

From linear algebra[24], we have

Theorem 1 (Legendre basis). *A polynomial given by*

$$V_n(x) = c_0 + c_1 x + c_2 x^2 + \ldots + c_n x^n$$

can be expanded into the first $n+1$ Legendre polynomials $L_0(x), \ldots, L_n(x)$, which provide a complete basis for the knot polynomial space $\mathcal{V}_n^+$.

Let us identify the adapted Jones polynomial $V_K(x)$ with $V_n(x)$, and apply Theorem 1; we have

$$V_K(x) = V_n(x) = c_0 L_0(x) + c_1 L_1(x) + c_2 L_2(x) + \ldots + c_n L_n(x), \qquad (7)$$

with

$$c_i = \int_{-1}^{1} V_n(x) L_i(x) \, dx \qquad (i = 0, 1, 2, \ldots, n), \qquad (8)$$

and $c_i = 0$ for all $i > n$. The coordinates of a point in $\mathcal{V}_n^+$ are thus given by $V_K(x) = (c_0, c_1, c_2, \ldots, c_n)$. Since from ref. [18] we have that $x \in [1, e]$, we must perform a change of variable to transform the interval $[1, e] \to [-1, 1]$; this is done by taking

$$x \to x' = \frac{2}{e-1} x - \frac{1+e}{e-1}, \qquad (9)$$

that gives

$$\int_{1}^{e} f[V_n(x)] \, dx = \frac{2}{e-1} \int_{-1}^{1} f[V_n(x')] \, dx'. \qquad (10)$$

Definition 2 (Metric). *The distance $d_{ij}(V_{K_i}, V_{K_j})$ in $\mathcal{V}_n^+$ between two points V_{K_i} and V_{K_j} determined by Eq. (7), is given by the Euclidean distance*

$$d_{ij} = \| V_{K_i} - V_{K_j} \| = \sqrt{\frac{2}{e-1}} \sqrt{\int_{-1}^{1} \left[V_{K_i}(x') - V_{K_j}(x') \right]^2 dx'}. \qquad (11)$$

Application to unlinking pathways. Let us apply Eq. (11) to the knot types of Fig. 3 to compute data for all possible unlinking pathways. For this we must compute the Legendre coordinates of all knots and links of Fig. 3 using Eq. (8). Numerical values are shown in Table 1, where actual values are computed with five precision digits. We identify 17 possible pathways shown in Fig. 4, including pathways through topological transitions $A \to T(2,5)$ and $B \to T(2,4)$ (denoted by long, dashed arrows in Fig. 4) that are not reported in the diagram of Fig. 3. The 17 possible pathways from $T(2,6)$ to the unknot $T(2,1)$ are described in Table 2.

The distance between the farthest knot $T(2,6)$ and the unknot $T(2,1)$ is measured by the length $d_0 = d(\Pi_0)$ that determines the
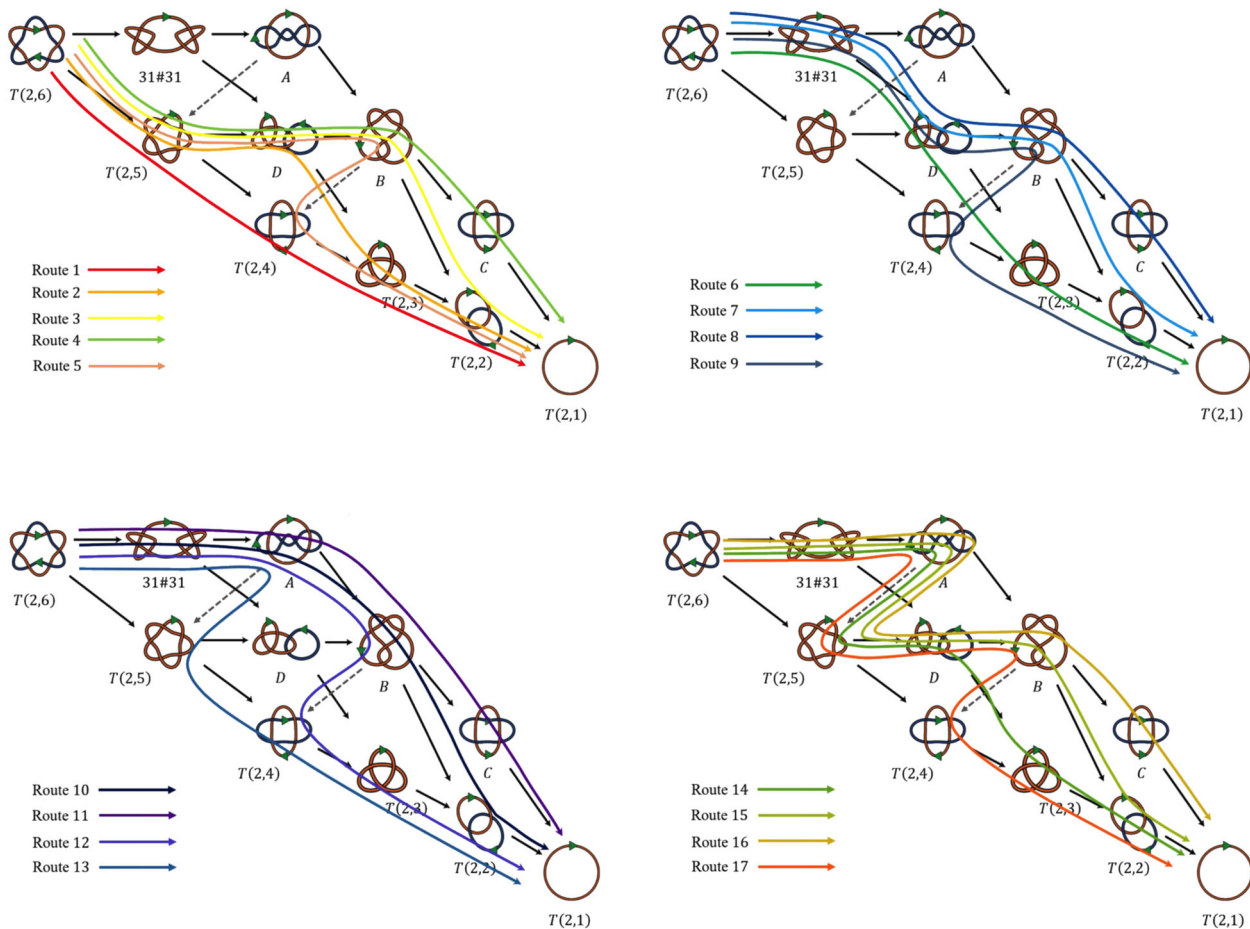
Fig. 4 Comparison between different decaying pathways. Possible routes of decaying pathways from $T(2,6)$ to $T(2,1)$, color coded according to the legends. Each torus knot/link is denoted by $T(p,q)$, where the numbers p and q denote, respectively, the number of longitudinal and meridian wraps of the knot/link type on the mathematical torus. Knot/link representatives denoted by A–D correspond to the Thistlethwaite link notation $L6a1$ (mirror), 5_2, $L4a1$ (anti-parallel), and $T(2,3)\#L2a1$ in the Rolfsen table; $Lc_{min}a1$ stands for link with topological crossing number c_{min} in table position 1, 5_2 denotes knot with topological crossing number $c_{min} = 5$ in table position 2, and $T(2,3)\#L2a1$ the connected sum of trefoil knot (the first torus knot) $T(2,3)$ and Hopf link (the first torus link) $L2a1$, also denoted by $T(2,2)$; 31#31 denotes the composite knot made of two trefoil knots $T(2,3)$ (see ref. [28] for standard knot table and notations). Green arrows denote strand orientation, long black arrows topological transitions due to single reconnection events. Long, dashed arrows indicate topological transitions due to single reconnection events not reported in ref. [2].

direct path Π_0 from $T(2,6)$ to $T(2,1)$, i.e.

$$d_0 = d(V_{T(2,6)} - V_{T(2,1)}) = d(V_{T(2,6)} - 1). \qquad (12)$$

From Table 1, we have $d_0 = 6.35193 \times 10^6$. The length $d_i = d(\Pi_i)$ of each route Π_i ($i = 1, \ldots, 17$) is given by the sum of the direct distances between knot pairs present in each route Π_i. In order to compare pathway lengths it is useful to introduce a non-dimensional measure given by the relative deviation σ_i of each Π_i from the direct route Π_0. This is given by $\sigma_i = (d_i - d_0)/d_0$.

We want to compute the probability associated with each route and compare the results with those of Stolz et al.[2]. Keeping in mind the cascade scenarios discussed in the Introduction, we may simply relate pathway length to probability by identifying shortest paths with most probable routes. An elementary definition of probability $p_i = p(\Pi_i)$ is thus given by taking p_i inversely proportional to σ_i; we have

$$p_i = \frac{\sigma_i^{-1}}{\sum_{k=1}^{17} \sigma_k^{-1}}, \qquad \sum_{i=1}^{17} p_i = 1. \qquad (13)$$

Numerical values of total length d_i, deviation σ_i and relative probability p_i are given in Table 3.

For the sake of example let's compute the probability associated with the transition $T(2,6) \to T(2,5)$: this is part of five routes, Π_1, Π_2, Π_3, Π_4, and Π_5 (see Fig. 4). Taking data from Table 3, we have

$$\begin{aligned} P_{T(2,6) \to T(2,5)} &= P(\Pi_1 \cup \Pi_2 \cup \Pi_3 \cup \Pi_4 \cup \Pi_5)|_{T(2,6) \to T(2,5)} \\ &= 97.6203\% + 0.622067\% + 0.454444\% \\ &\quad + 0.45440\% + 0.454399\% \\ &\approx 99.6\%. \end{aligned}$$

Similarly for the computation of other probabilities associated with each transition. The results, shown in red in Fig. 5, are juxtaposed with those (in black) obtained by Stolz et al. As we see the comparison is very satisfactory, especially if we take into account the rate of change of each single transition (not shown).

It is interesting to compare deviations, relative probabilities, and topological complexity of the routes examined. In Fig. 6 we show (panel a) the plot of deviations and (panel b) the relative probabilities against Π_i. As we see, deviations cluster into four, well separated sets identified by encircled

Table 2 Possible routes to decaying pathways in the decay from $T(2,6)$ to $T(2,1)$.

Route	Pathway
Π_1 :	$T(2,6) \rightarrow T(2,5) \rightarrow T(2,4) \rightarrow T(2,3) \rightarrow T(2,2) \rightarrow T(2,1)$
Π_2 :	$T(2,6) \rightarrow T(2,5) \rightarrow D \rightarrow T(2,3) \rightarrow T(2,2) \rightarrow T(2,1)$
Π_3 :	$T(2,6) \rightarrow T(2,5) \rightarrow D \rightarrow B \rightarrow T(2,2) \rightarrow T(2,1)$
Π_4 :	$T(2,6) \rightarrow T(2,5) \rightarrow D \rightarrow B \rightarrow C \rightarrow T(2,1)$
Π_5 :	$T(2,6) \rightarrow T(2,5) \rightarrow D \rightarrow B \rightarrow T(2,4) \rightarrow T(2,3) \rightarrow T(2,2) \rightarrow T(2,1)$
Π_6 :	$T(2,6) \rightarrow 31\#31 \rightarrow D \rightarrow T(2,3) \rightarrow T(2,2) \rightarrow T(2,1)$
Π_7 :	$T(2,6) \rightarrow 31\#31 \rightarrow D \rightarrow B \rightarrow T(2,2) \rightarrow T(2,1)$
Π_8 :	$T(2,6) \rightarrow 31\#31 \rightarrow D \rightarrow B \rightarrow C \rightarrow T(2,1)$
Π_9 :	$T(2,6) \rightarrow 31\#31 \rightarrow D \rightarrow B \rightarrow T(2,4) \rightarrow T(2,3) \rightarrow T(2,2) \rightarrow T(2,1)$
Π_{10} :	$T(2,6) \rightarrow 31\#31 \rightarrow A \rightarrow B \rightarrow T(2,2) \rightarrow T(2,1)$
Π_{11} :	$T(2,6) \rightarrow 31\#31 \rightarrow A \rightarrow B \rightarrow C \rightarrow T(2,1)$
Π_{12} :	$T(2,6) \rightarrow 31\#31 \rightarrow A \rightarrow B \rightarrow T(2,4) \rightarrow T(2,3) \rightarrow T(2,2) \rightarrow T(2,1)$
Π_{13} :	$T(2,6) \rightarrow 31\#31 \rightarrow A \rightarrow T(2,5) \rightarrow T(2,4) \rightarrow T(2,3) \rightarrow T(2,2) \rightarrow T(2,1)$
Π_{14} :	$T(2,6) \rightarrow 31\#31 \rightarrow A \rightarrow T(2,5) \rightarrow D \rightarrow T(2,3) \rightarrow T(2,2) \rightarrow T(2,1)$
Π_{15} :	$T(2,6) \rightarrow 31\#31 \rightarrow A \rightarrow T(2,5) \rightarrow D \rightarrow B \rightarrow T(2,2) \rightarrow T(2,1)$
Π_{16} :	$T(2,6) \rightarrow 31\#31 \rightarrow A \rightarrow T(2,5) \rightarrow D \rightarrow B \rightarrow C \rightarrow T(2,1)$
Π_{17} :	$T(2,6) \rightarrow 31\#31 \rightarrow A \rightarrow T(2,5) \rightarrow D \rightarrow B \rightarrow T(2,4) \rightarrow T(2,3) \rightarrow T(2,2) \rightarrow T(2,1)$

Π_i indicates the ith decaying route associated with the ith pathway ($i = 1, \dots, 17$, where i denotes the path number). Each torus knot/link is denoted by $T(p,q)$, where the numbers p and q denote respectively the number of longitudinal and meridian wraps of the knot/link type on the mathematical torus. Knot/link representatives denoted by A–D correspond to the Thistlethwaite link notation $L6a1$ (mirror), 5_2, $L4a1$ (anti-parallel) and $T(2,3)\#L2a1$ in the Rolfsen table; $Lc_{min}a1$ stands for link with topological crossing number c_{min} in table position 1, 5_2 denotes knot with topological crossing number $c_{min} = 5$ in table position 2, and $T(2,3)\#L2a1$ the connected sum of trefoil knot (the first torus knot) $T(2,3)$ and Hopf link (the first torus link) $L2a1$, also denoted by $T(2,2)$; $31\#31$ denotes the composite knot made of two trefoil knots $T(2,3)$ (see ref. [28] for standard knot table and notations).

Table 3 Length, deviation and probability of the 17 routes considered in the decay from $T(2,6)$ to $T(2,1)$.

Route	d_i	$d_i - d_0$	σ_i	p_i [%]
Π_0	6.35193×10^6	–	–	–
Π_1	6.3536331×10^6	1.70041×10^3	2.67699×10^{-4}	97.6203
Π_2	6.6187759×10^6	2.66843×10^5	4.20098×10^{-2}	0.622067
Π_3	6.7172016×10^6	3.65269×10^5	5.75052×10^{-2}	0.454444
Π_4	6.7172366×10^6	3.65304×10^5	5.75107×10^{-2}	0.45440
Π_5	6.7172370×10^6	3.65305×10^5	5.75108×10^{-2}	0.454399
Π_6	1.0359563×10^7	4.00763×10^6	6.30931×10^{-1}	0.0414196
Π_7	1.0457989×10^7	4.10606×10^6	6.46426×10^{-1}	0.0404267
Π_8	1.0458024×10^7	4.106092×10^6	6.46432×10^{-1}	0.04042634
Π_9	1.0458025×10^7	4.106093×10^6	6.46432×10^{-1}	0.04042633
Π_{10}	1.1918964×10^7	5.56703×10^6	8.76431×10^{-1}	0.0298174
Π_{11}	1.1918999×10^7	5.567066×10^6	8.764366×10^{-1}	0.029817188
Π_{12}	1.1919000×10^7	5.567067×10^6	8.764368×10^{-1}	0.029817184
Π_{13}	1.1919344×10^7	5.56741×10^6	8.76491×10^{-1}	0.0298153
Π_{14}	1.2184486×10^7	5.83255×10^6	9.18233×10^{-1}	0.02846
Π_{15}	1.2282912×10^7	5.93098×10^6	9.33728×10^{-1}	0.0279877
Π_{16}	1.2282947×10^7	5.93101×10^6	9.337338×10^{-1}	0.02798750
Π_{17}	1.2282948×10^7	5.93102×10^6	9.337340×10^{-1}	0.02798749

Π_0 indicates the route associated with the direct path between $T(2,6)$ and $T(2,1)$ of length d_0; Π_i ($i = 1, \dots, 17$, where i denotes the path number) indicates the ith decaying route associated with the ith pathway; d_i indicates the length of the route Π_i, $d_i - d_0$ the difference between d_i and the length d_0 of the direct path between $T(2,6)$ and $T(2,1)$, $\sigma_i = (d_i - d_0)/d_0$ the relative deviation, p_i the relative probability.

regions. This clustering reflects the group of pathways shown in the diagrams of Fig. 4. Note that the deviation of Π_1 from Π_0 is as small as 0.0268%, two orders of magnitude smaller than σ_2; the probability of Π_1 is $p_1 = 97.6\%$ (Fig. 6b), proving to be by far the most probable route among all possible routes.

As far as topological complexity is concerned, we introduce a new complexity measure in terms of distance between points in $\mathcal{V}_n^+$ and the unknot making use of Eq. (11). Since the unknot has $V_{T(2,1)} = 1$ and knot complexity tends to increase exponentially with the topological crossing number c_{min}, it is useful to provide a new definition of topological complexity in terms of natural logarithm.

Definition 3 (Complexity degree). The topological complexity of a knot K is defined by the complexity degree $\chi(K)$ given by

$$\chi(K) = \ln\left[1 + d\left(V_K, V_{T(2,1)}\right)\right]. \tag{14}$$

The plot $\chi = \chi(K)$ for data extracted from Table 1 is shown in Fig. 7. The superposed dashed line is a best-fit curve given by $\chi = 6.3 \ln K - 0.13$, where K denotes the knot/link present in Fig. 3. Since for increasing complexity we have a logarithmic growth in terms of c_{min}, this is consistent with the usual assumption that the number of knot/link types must increase exponentially with c_{min}.
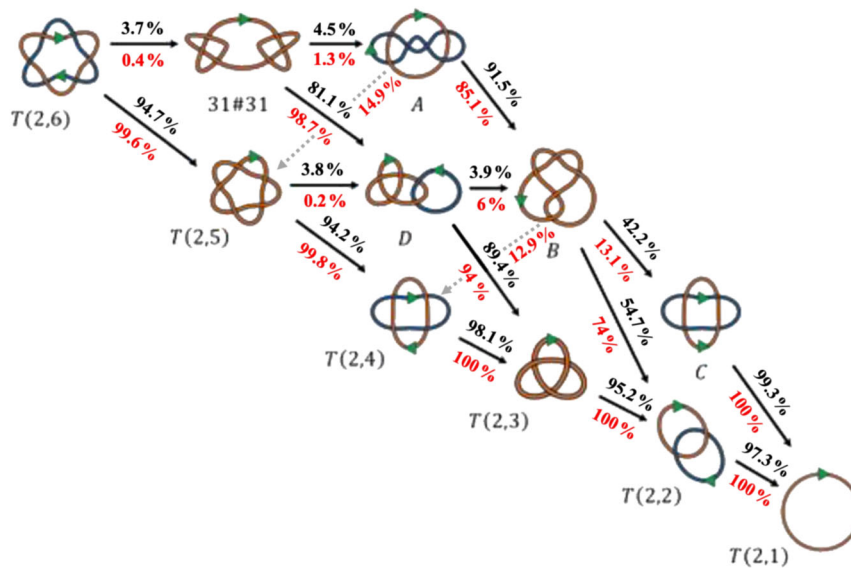
Fig. 5 Comparative analysis of transition probability values. Probability values obtained by Stolz et al.[2] (in black) juxtaposed with the ones in red obtained by the present method. Each torus knot/link is denoted by $T(p,q)$, where the numbers p and q denote, respectively, the number of longitudinal and meridian wraps of the knot/link type on the mathematical torus. Knot/link representatives denoted by A–D correspond to the Thistlethwaite link notation $L6a1$ (mirror), 5_2, $L4a1$ (anti-parallel), and $T(2,3)\#L2a1$ in the Rolfsen table; $Lc_{min}a1$ stands for link with topological crossing number c_{min} in table position 1, 5_2 denotes knot with topological crossing number $c_{min} = 5$ in table position 2, and $T(2,3)\#L2a1$ the connected sum of trefoil knot (the first torus knot) $T(2,3)$ and Hopf link (the first torus link) $L2a1$, also denoted by $T(2,2)$; $31\#31$ denotes the composite knot made of two trefoil knots $T(2,3)$ (see ref. [28] for standard knot table and notations). Green arrows denote strand orientation, long black arrows topological transitions due to single reconnection event. The additional transitions $A \to T(2,5)$ and $B \to T(2,4)$ denoted by dashed arrows represent also topological transitions due single reconnection events and are not reported by Stolz et al. [2]; these additional transitions determine some small corrections in the overall assessment of transition probabilities.
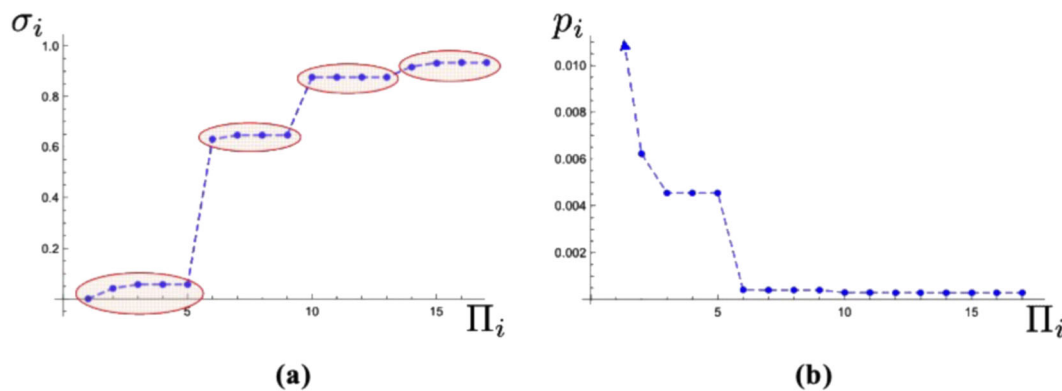

Fig. 6 Deviation and relative probability of the 17 routes examined. a Relative deviation σ_i ($i = 1, \ldots, 17$ denotes pathway number); σ_i values cluster into four, well separate sets identified by the encircled regions. **b** Probability p_i of each route Π_i. The first route Π_1 has probability $p_1 = 97\%$, which is several orders of magnitude larger than the probability of all other pathways.

Discussion

It is natural to ask whether the topological simplification analyzed here can be put in any relation with typical energy cascade processes observed in nature. The logarithmic best-fit curve of Fig. 7 is extrapolated from purely topological data, without any reference to physical or biological processes. A physical justification of this logarithmic growth, however, can be given by comparing these results with data obtained from the analysis of minimum energy states of magnetic knots and links[21] and, to some extent, of elastic systems[22]. By examining the numerical values of the groundstate spectra determined there we can see that energy minima grow with topological complexity as $a \ln \#_K + b$, with a and b constants (and independent of knot types), and $\#_K$ denoting knot tabulation according to increasing ropelength λ. Note that $\lambda(\#_K) \propto c_{min}^{3/4}$ (ref. [21], Eq. (19)). This comparison shows a

remarkable similarity between logarithmic growths. Since magnetic minima are magneto-hydrodynamic configurations that represent also steady states of Euler flows[25–27], one can interpret those minima as energy lower bound representatives of *any* pathway cascade associated with energy reduction, be it due to elastic relaxation, viscous dissipation, or quantum effects. Hence, it is not so surprising to observe that any of the 17 routes considered above fits into the logarithmic decay of Fig. 7. It is also worth noticing that the best-fit curve of the optimal geodesic given by the most probable sequence Π_1 is arguably the closest match to the best-fit behavior obtained in ref. [21].

In summary, a new way to analyze and interpret optimal pathways attained through topological simplification of physical knots and links by step-wise sequence of unlinking events, such as those studied by Stolz et al.[2], is introduced and tested. This is
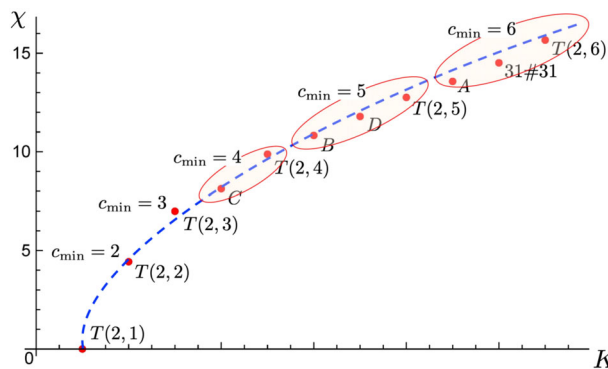
Fig. 7 Complexity degree of knots and links. Complexity degree χ (defined by Eq. (14)) plotted against knots and links K in pathways $\Pi_1, \ldots, \Pi_{17}$. Each torus knot/link is denoted by $T(p,q)$, where the numbers p and q denote, respectively, the number of longitudinal and meridian wraps of the knot/link type on the mathematical torus. Knot/link representatives denoted by A–D correspond to the Thistlethwaite link notation $L6a1$ (mirror), 5_2, $L4a1$ (anti-parallel), and $T(2,3)\#L2a1$ in the Rolfsen table; $Lc_{min}a1$ stands for link with topological crossing number c_{min} in table position 1, 5_2 denotes knot with topological crossing number $c_{min} = 5$ in table position 2, and $T(2,3)\#L2a1$ the connected sum of trefoil knot (the first torus knot) $T(2,3)$ and Hopf link (the first torus link) $L2a1$, also denoted by $T(2,2)$; $31\#31$ denotes the composite knot made of two trefoil knots $T(2,3)$ (see ref. [28] for standard knot table and notations). Best-fit curve (dashed) is given by $\chi = 6.3 \ln K - 0.13$; encircled regions identify knots and links of same topological crossing number c_{min}.

done by relying on Arnold's original idea of interpreting an evolutionary process as geodesic in an appropriate metric space. For this we introduce a discrete knot polynomial space whose points are defined by knot polynomials. Here we consider the adapted Jones polynomials introduced by Liu and Ricca[18], identifying knot coordinates by Legendre polynomials. By defining an appropriate orthonormal metric, we apply this method to analyze the last stages of the unlinking pathways studied by Stolz et al.[2] in terms of discrete geodesic flows, and for each topological transition we compute the relative probability. The results obtained match very well the data obtained in ref. [2] without using any extra assumption other than complexity reduction by stepwise unlinking. Moreover, by introducing a new measure of topological complexity based on distances in the knot space, we show that optimal decaying pathways observed in various physical systems in nature are well captured by a logarithmic best-fit curve that is functionally related, and bounded from below, by the logarithmic distribution of minimum energy states of tight physical knots[21,22].

All in all this new approach proves to be rather powerful and flexible. The use of a knot polynomial space through the computation of point coordinates by direct application of Eq. (8) allows one to explore topological unlinking pathways more complex than the ones analyzed here. Moreover, the new measure of complexity degree (a scalar quantity) defined by Eq. (14) can be straightforwardly applied to sample and predict admissible pathways before any detailed evaluation of probability routes using this measure as an exclusion principle, by exploiting the fact that any admissible pathway generates a monotonically decreasing sequence of χ-values. Finally, a conjecture about energy-complexity relations: since the considerations above are independent from any specific physical process, it would seem plausible to assume that any minimal simplification process could yield structural simplification governed by a logarithmic decrease proportional to topological complexity. If so, this would suggest an intriguing connection between topological simplification and

energy cascade and entropy production. In this regard the novel approach proposed here seem to have great potential for future investigations.

Data availability

References

1. Shimokawa, K., Ishihara, K., Grainge, I., Sherratt, D. J. & Vazquez, M. FtsK-dependent XerCD-dif recombination unlinks replication catenanes in a stepwise manner. *Proc. Natl. Acad. Sci. USA* **110**, 20906–20911 (2013).
2. Stolz, R., Yoshida, M., Brasher, R., Flanner, M. & Ishihara, K. et al. Pathways of DNA unlinking: a story of stepwise simplification. *Sci. Rep.* **7**, 12420 (2017).
3. Kleckner, D. & Irvine, W. T. M. Creation and dynamics of knotted vortices. *Nat. Phys.* **9**, 253–258 (2013).
4. Proment, D., Onorato, M. & Barenghi, C. F. Vortex knots in a Bose–Einstein condensate. *Phys. Rev. E* **85**, 1 (2012).
5. Zuccher, S. & Ricca, R. L. Relaxation of twist helicity in the cascade process of linked quantum vortices. *Phys. Rev. E* **95**, 053109 (2017).
6. Kleckner, D., Kauffman, L. H. & Irvine, W. T. M. How superfluid vortex knots untie. *Nat. Phys.* **9**, 253–258 (2016).
7. Cooper, R. G., Mesgarnezhad, M., Baggaley, A. W. & Barenghi, C. F. Knot spectrum of turbulence. *Sci. Rep.* **9**, 10545 (2019).
8. Sumners, De. W. L. Lifting the curtain: using topology to probe the hidden action of enzymes. *Not. Am. Math. Soc.* **42**, 528–537 (1995).
9. Priest, E. & Forbes, T. *Magnetic Reconnection*. (Cambridge University Press, Cambridge, 2000).
10. van Rees, W., Hussain, F. & Koumoutsakos, P. Vortex tube reconnection at Re = 104. *Phys. Fluids* **24**, 075105 (2012).
11. Bewley, G., Paoletti, M. S., Sreenivasan, K. R. & Lathrop, D. P. Characterization of reconnecting vortices in superfluid helium. *Proc. Natl Acad. Sci. USA* **105**, 13707–13710 (2008).
12. Zuccher, S., Caliari, M., Baggaley, A. W. & Barenghi, C. F. Quantum vortex reconnection. *Phys. Fluids* **24**, 1251081 (2012).
13. Laing, C. E., Ricca, R. L. & Sumners De, W. L. Conservation of writhe helicity under anti-parallel reconnection. *Sci. Rep.* **5**, 9224 (2015).
14. Liu, X. & Ricca, R. L. Knots cascade detected by a monotonically decreasing sequence of values. *Sci. Rep.* **6**, 24118 (2016).
15. Rolfsen, D. *Knots and Links*. (Publish or perish Inc., Berkeley, 1976).
16. Kauffman, L. H. *Knots and Physics*. (World Scientific, Singapore, 2001).
17. Arnold, V. I. & Khesin, B. A. *Topological Methods in Hydrodynamics*. (Springer-Verlag, New York, 1998).
18. Liu, X. & Ricca, R. L. The Jones polynomial for fluid knots from helicity. *J. Phys. A* **45**, 205501 (2012).
19. Liu, X. & Ricca, R. L. On the derivation of HOMFLYPT polynomial invariant for fluid knots. *J. Fluid Mech.* **773**, 34–48 (2015).
20. Moffatt, H. K. The energy spectrum of knots and links. *Nature* **34**, 367–369 (1990).
21. Ricca, R. L. & Maggioni, F. On the groundstate energy spectrum of magnetic knots and links. *J. Phys. A* **47**, 205501 (2014).
22. Ricca, R. L. & Maggioni, F. Groundstate energy spectra of knots and links: magnetic versus bending energy. In *New Directions in Geometric and Applied Knot Theory. OA Measure Theory* (eds Blatt, S., Reiter, P. & Schikorra, A.), 276–288 (De Gruyter, Basel, 2018).
23. Andrews, G.E., Askey, R. & Roy, R. *Special Functions. Encyclopedia of Mathematics and its Applications*. Vol. 71 (Cambridge University Press, Cambridge, 1999).
24. Leon, S. *Linear Algebra with Applications*. (Pearson Education Inc., London, 2010).
25. Arnold, V. I. Sur un principle variationnel pour les ecoulements stationnaires des liquides parfaits et ses applications aux problems de stabilité non-lineaires. *J. Mec.* **5**, 29–43 (1966).
26. Moffatt, H. K. Magnetostatic equilibria and analogous Euler flows of arbitrarily complex topology. Part I, Fundamentals. *J. Fluid Mech.* **159**, 359–378 (1985).
27. Moffatt, H. K. Relaxation under topological constraints. In *Topological Aspects of the Dynamics of Fluids and Plasmas* (eds Moffatt, H. K., Zaslavsky, G. M., Comte, P. & Tabor, M.), 3–28 (Kluwer Academic Publishers, Dordrecht, 1992).
28. The Knot Atlas. http://katlas.org/wiki/Main_Page (2015).

Author contributions

X.L. and R.L.R. devised the project, X.L. and X-F.L. performed computations and produced data, X.L. and R.L.R. wrote the paper. All the authors contributed to revision equally.

Competing interests

The authors declare no competing interests.

Additional information

Supplementary information is available for this paper at https://doi.org/10.1038/s42005-020-00398-y.

Correspondence and requests for materials should be addressed to R.L.R.

Reprints and permission information is available at http://www.nature.com/reprints

Publisher's note Springer Nature remains neutral with regard to jurisdictional claims in published maps and institutional affiliations.